Since January 2020 Elsevier has created a COVID-19 resource centre with free information in English and Mandarin on the novel coronavirus COVID-19. The COVID-19 resource centre is hosted on Elsevier Connect, the company's public news and information website.

Journal of Pharmaceutical and Biomedical Analysis 221 (2022) 115057

Contents lists available at ScienceDirect

Journal of Pharmaceutical and Biomedical Analysis

journal homepage: www.journals.elsevier.com/journal-of-pharmaceutical-and-biomedical-analysis

A novel and water-soluble material for coronavirus inactivation from oseltamivir in the cavity of methyl and sulfated-β-cyclodextrins through inclusion complexation

Rajaram Rajamohan [a,*], Sonaimuthu Mohandoss [a], Sekar Ashokkumar [b], Fatiha Madi [c], Neour Leila [c], Kuppusamy Murugavel [d], Yong Rok Lee [a,*]

[a] School of Chemical Engineering, Yeungnam University, Gyeongson 38541, Republic of Korea
[b] PBRC Research center, Kwangwoon University, Seoul 01897, Republic of Korea
[c] Laboratory of Computational Chemistry and Nanostructures, Department of Material Sciences, Faculty of Mathematical, Informatics and Material Sciences, University of 8 May 1945, Guelma, Algeria
[d] PG and Research Department of Chemistry, Government Arts College, Chidambaram 608102, India

ARTICLE INFO

Keywords:
Oseltamivir
Modified cyclodextrins
Water-soluble inclusion materials
Drug delivery
Coronavirus inactivation

ABSTRACT

A potentially active water-soluble anti-viral with lesser toxic material from the Oseltamivir (OTV) has been produced by the sonication method. The formed material has been further characterized by UV–visible, FT-IR, powder XRD, SEM, TGA/DTA, ROESY, XPS, AFM and etc., The results of DFT calculation have proven that inclusion complexes (ICs) are theoretically and energetically more advantageous models and structures have also been proposed based on the results. Analysis of drug release has been carried out at three pH levels, and it is revealed the analysis is most helpful at acidic pH levels for the ICs with S-CD over H-CD. Over OTV without CDs, OTV:S-CD-ICs exhibited a very less cytotoxic ability on cancer cell lines than ICs with M-CD. ICs enhanced the coronavirus inactivation nature of OTV. This study provides for the first time a full characterization of ICs of OTV with CDs and highlights the impact of complexation on pharmacological activity.

1. Introduction

The cyclic oligosaccharides cyclodextrins (CDs) are composed of six, seven, or eight D-glucopyranosyl units and are designated as α-CD, β-CD, and γ-CD, respectively. The molecules are doughnut-shaped with hydrophilic surfaces on the outside and somewhat hydrophobic interiors. Inclusion complexes (ICs) are formed with a wide variety of compounds (guests) when a lipophilic moiety of the guest molecule is taken up into the cavity of the CD (host) molecule, increasing the solubility and stability of the guest in water [1–6].

In some studies, low-water-soluble drugs have been enhanced in solubility after making them into ICs by the non-covalent bonding interaction between the drug and CD [7–10]. It is extremely difficult to make water-soluble ICs for the drug with CDs [11,12]. It is expected that fullerene-based water-soluble ICs made with CDs would be a good material for a variety of medical applications [13]. ICs made from easily water-soluble materials are always being highlighted in supramolecular assembly and require this material for both virology and drug delivery. The derivatives of CDs like methylated and sulfated CDs have been chosen here to get a powerful anti-viral agent against HCoV-229E because both the derivatives have easily water-soluble than the other derivatives [4].

There may be antiviral drugs, as well as different drugs and also drug combinations that are effective in treating the current coronavirus

Abbreviations: OTV, Oseltamivir; M-CD, Methylated-β-Cyclodextrin; S-CD, Sulfated-β-Cyclodextrin; UV, Ulta-Violet; FT-IR, Fourier Transform - Infra Red spectroscopy; powder XRD, Powder X-Ray Diffraction; FE-SEM, Field Emission Scanning Electron Microscopy; EDAX, Energy Dispersive X-Ray Analysis; AFM, Atomic Force Microscopy; TGA, Therogravimetric Analaysis; DTA, Differential Thermal Analysis; 1 H NMR, Proton Nuclear Magnetic resonance spectroscopy; ROESY, Rotating Frame Overhauser Enhancement Spectroscopy; XPS, X-ray Photoelectron spectroscopy; DFT, Density Functional Theory; CD, Cyclodextrin; CDs, Cyclodextrins; EDTA, Ethylene-di-aminetetraacetic acid; IC, Inclusion Complex; ICs, Inclusion Complexes; K_b, Binding Constant; C, Celsius; eV, electron volt; ppm, parts per million; nm, nanometer; HOMO, Highest energy Occupied Molecular Orbital; LUMO, Lowest energy Unoccupied Molecular Orbital; CPE, Cytopathic effect; $TCID_{50}$, Tissue Culture Infectious Dose.

* Corresponding authors.
E-mail addresses: rajmohanau@yu.ac.kr (R. Rajamohan), yrlee@yu.ac.kr (Y.R. Lee).

https://doi.org/10.1016/j.jpba.2022.115057
Received 15 August 2022; Received in revised form 12 September 2022; Accepted 14 September 2022
Available online 15 September 2022

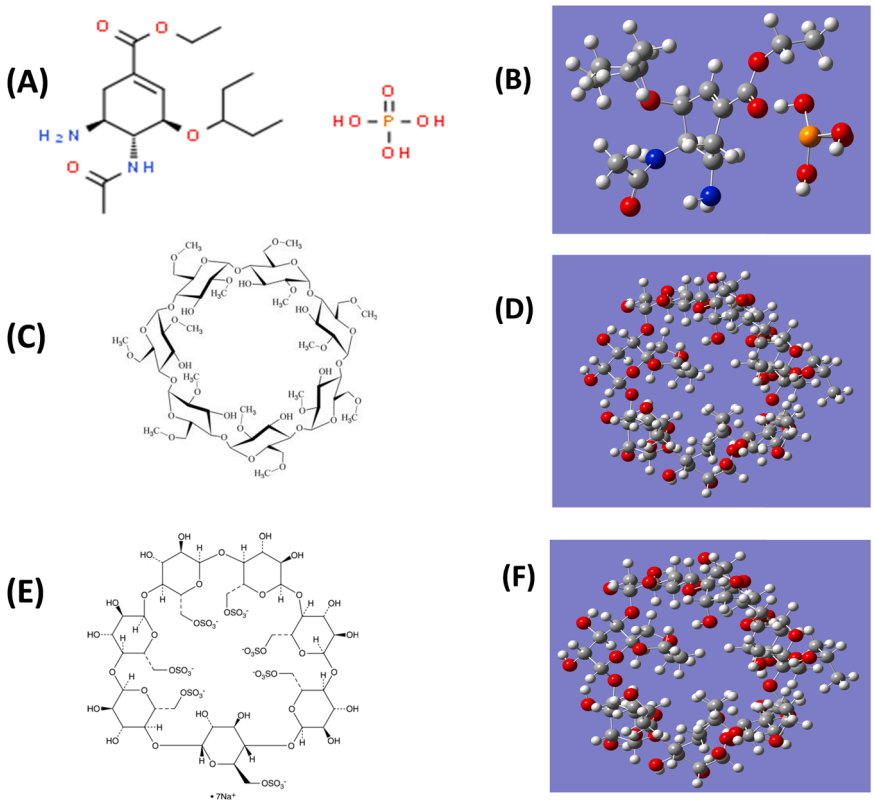

Fig. 1. Structures of the naturally occurring (A & B) OTV, (C & D) M-CD and (E & F) S-CD.

pandemic. The effectiveness of OTV in the prevention of H_5N_1 infection [14] and COVID-19 infection [15] has been extensively studied in clinical trials. Several carriers are used in drug discovery to test existing antiviral drugs that are used to treat other viral infections. Drug discovery approaches are usually combined with this approach to identify drug compounds that can be categorized as virus-based and host-based treatments during emerging COVID-19 outbreaks. We have chosen OTV as the antiviral drug and we have tested it for both viral activity and CDs as the means of reaching the viral inactivation destination, as well as its low toxicity during operation.

Our goal is to prepare and characterize OTV ICs using M-CDs and S-CDs in this research. In order to inactivate viruses using these ICs, we are primarily interested in exploring drug delivery. A major focus of our research will be to explore the use of these water-soluble ICs as antiviral agents. Phase solubility studies are conducted to determine the solubility and also to determine the binding constant. Ultrasonication is used to prepare the solid-state complexes. These ICs are characterized using a variety of techniques. By using the Alamar Blue assay, toxic behavior has been tested against the MRC-5 cell line. Inactivation of the virus has been carried out on ICs containing HCoV-229E.

2. Materials and methods

2.1. Materials

OTV (Formula - $C_{16}H_{28}N_2O_4{\cdot}H_3PO_4$, Purity - ≥98%) and substituted CDs (Methyl-β-Cyclodextrin (M-CD): Formula - $C_{54}H_{94}O_{35}$, Molecular Weight - 1303.3, purity - 99.95%; & Sulfated-β-Cyclodextrin (S-CD): Formula - $C_{42}H_{70}O_{56}S_7$, Molecular Weight - 1849.5, purity - 99.85%) are supplied by Sigma-Aldrich, South Korea. Distilled water is used during the entire study. Assays can be conducted using products from Sigma Aldrich, St Louis, USA, Fetal Bovine Serum (FBS), Phosphate Buffered Saline (PBS), Dulbecco's Modified Eagle's Medium (DMEM), and Trypsin. Dimethyl sulfoxide (DMSO) and propanol are supplied by E-Merck Ltd., Korea. Fig. 1 illustrates the structure of the guest, OTV, host, M-CD and S-CD. MRC-5 human lung fibroblast host cells are purchased from the Korean Cell Line Bank (KCLB, Seoul, Korea), and HCoV-229E is obtained from the ATCC, Manassas, VA, USA.

2.2. Preparation of ICs of OTV with M-CD and S-CD

A sonication method and freeze-drying technique are used to prepare ICs of OTVs with CDs. The sonication process is so very simple and time-consuming to get the product. Briefly, we synthesized both OTV ICs with M-CD and S-CD using an ultrasonic device, a Hielsher UP200St. In order to prepare the ICs, a solution of OTV with 0.044 M is added dropwise to the solutions of M-CD and S-CD with 0.044 M separately (to get the 1:1 molar ratio of host-guest combinations). Continually stirring the mixture with a magnetic field heated it to 60 °C. Ultrasonic devices Hielsher UP200ST are used to sonicate the solution for 90 min (2 sets of 300 s each). As the entire solution appears clear, the ICs are water-soluble. Watery removal has therefore been employed. After each solution has been frozen-dried at − 82 °C for 48 h, the white powers are collected as complexes of OTV:M-CD (ICs-1) and OTV:S-CD (ICs-2). This method saves both time and energy.

2.3. Phase solubility measurements

In order to determine the solubility of OTV in the aqueous phase of CDs, phase solubility (PS) measurements are performed using the modification of Higuchi et al. [16]. As a brief summary, aqueous solutions of M-CD and S-CD of concentrations of 0–12 mM in phosphate buffer (10 mM; pH 7.4) are prepared after OTV is excessively added. Flasks are covered with aluminum foil to prevent photochemical degradation. First, the solutions are sonicated in an ultrasonic bath (30 kHz, 100 W, SAIRAN Micro10sonic, Korea) at 25 °C for an hour, then 48 h is allowed for equilibrium to develop. The aqueous solutions are centrifuged for 10 min at 8000 rpm, then allowed to cool. We

cleaned the obtained supernatants by filtering them through membrane filters of 0.2 μm and analyzing them with a UV–vis spectrophotometer (Jasco, V-630, Tokyo, Japan) to remove any undissolved solids. According to Eqs. 1 and 2, the binding constant (K_b) of OTV:M-CD-ICs and OTV:S-CD-ICs can be determined by the slope and intercept of the straight line of the phase solubility diagram [17]:

$$K_b = \frac{slope}{S_0(1 - slope)} \quad (1)$$

$$\mathrm{CE} = \frac{slope}{(1 - slope)} \quad (2)$$

Here, S_0 is the intrinsic solubility of OTV.

2.4. DFT Inputs

Hyperchem [18] is used to construct the initial structure of OTV. Chem-Office 3D ultra (version 10, Cambridge software) is used to implement the first geometry of M-CD and S-CD. Afterward, they are optimized by a semi-empirical PM6-DH+ calculation, which, in many cases, yields interaction energies comparable to those derived by Density Functional Theory (DFT) [19]. According to Fatiha, et al., [20], the ICs of OTV in CDs are also controlled by PM6-DH+ calculations based on the A and B orientations. Thereafter, the PM6-DH+ structures with the lowest energy are optimized successively using the B3LYP/6–311 G (d, p) method. In order to verify that the obtained structures are global minimums, vibration frequencies are calculated.

2.5. Kinetic studies of in-vitro OTV release

Three different conditions of phosphate buffers (pH 5.2, 6.8, and 7.4) are tested at room temperature for the kinetic study of OTV release. The material is taken from a pre-prepared IC containing 10 mg/5 ml and placed into a dialysis membrane tube with a molecular cut-off of 12000 Da (Himedia, Dialysis membrane-110). After inserting the tubes into the buffer, 30 ml of PBS is poured into each tube. Every 2 ml from the release medium is replaced with a fresh PBS buffer. The amount of OTV released is measured spectrophotometrically by measuring the absorbance at 217.0 nm at different time intervals.

2.5.1. Reagents for cell viability and cytopathic assay

In the cell culture medium, Dulbecco's Modified Eagle Medium (DMEM, Sigma-Aldrich, Waltham, MA, USA), Fetal Bovine Serum (FBS, RDTech, Palatine, IL, USA), antibiotics (Welgene Inc., Gyeongsan, South Korea), and an HCoV-229E virus are obtained from the American Type Culture Collection (ATCC, Manassas, VA, USA) in combination with MRC- 5 cells. The Alamar Blue Assay (Invitrogen, Waltham, MA, USA) is used to determine cell cytotoxicity.

2.5.2. MRC-5 cell culture

To culture, the MRC-5 (human lungs fibroplast cell) cells, Dulbecco's Modified Eagle Medium (DMEM) supplemented with 10% fetal bovine serum and 1% antibiotics (streptomycin and penicillin) is used in a T-75 flask. For the cell viability test/$TCID_{50}$ experiment, the MRC-5 inoculated plates are incubated at 37 °C in 5% CO_2 for up to 2 days until the cells reached 80% confluence.

2.5.3. Cell viability assay

We performed a cytotoxicity assay using Alamar blue reagent in accordance with the manufacturer's instructions. MRC-5 cells (2×10^3 cells) are plated in 96-well plates and incubated at 37 °C with 5% CO_2 for 24 h to reach 80% confluence. Afterward, the cells are incubated for 7 days with different concentrations of OTV with CDs (OTV, OTV:M-CD-ICs, and OTV:S-CD-ICs). After removing the cell culture medium (time test), the cells are washed with DPBS. DMEM (without FBS and antibiotics) contain 100 μl of every concentration of CDs of 5.0, 0.5, 0.05, or

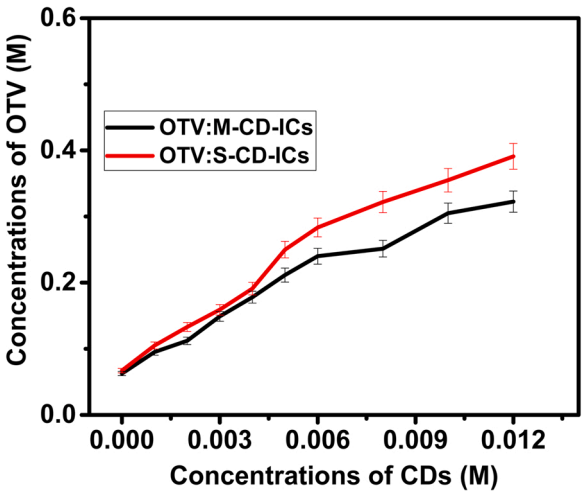

Fig. 2. Phase solubility diagram of ICs of OTV with CDs.

0.005 mg/ml for up to 7 days at 37 °C with 5% CO_2. The plate is incubated for up to two hours at 37 °C, 5% CO_2, and covered with protection against direct light based on diverse instance periods. A microplate reader Synergy HT spectrophotometer (BioTek, Winooski, VT, USA) is used to measure the absorbance values at 540.0 and 600.0 nm (excitation and emission wavelength, respectively).

2.5.4. Viral titration

A human coronavirus 229E ($1 \times 10^{6.5}$ $TCID_{50}$/ml) is inoculated into a MRC-5 cells (2×10^3 cells/well). Cells are suspended in DMEM enriched with 2% FBS containing 1 mg/ml of different OTV and ICs containing M-CD and S-CD. Each diluted test compound (100 μl) is tested in eight replicates, in which eight wells are used as negative controls (MRC-5 cells only) and eight more wells are used as positive controls (only HCoV-229E without OTV derivative). The plates are incubated at 37 °C, 5% CO_2 for 10 days and everyday observed expansion of the cytopathic effect (CPE). The CPE is calculated based on Reed and Muench [21].

2.6. Instruments used

The ICs are analyzed for their formation by various techniques such as UV–visible spectroscopy, FT-IR spectroscopy, Raman spectroscopy, FE-SEM along with EDX spectroscopy, AFM, powder XRD, TG/DTA, XPS, ^{1}H NMR and ROESY techniques. UV–vis spectra are performed within the ranges of 200.0–800.0 nm using OPTIZEN 3220 UV spectrophotometer with quartz cuvettes (1 cm path length) and a wavelength uncertainty is about ± 2.0 nm. The optimized wavelength scans are registered from 200.0 to 800.0 nm.

FT-IR spectra are recorded in the transmittance mode on a Perkin Elmer Spectrum Two within the range of wavenumbers (400.0–4000.0 cm^{-1}). FE-SEM along with EDX spectral analysis is carried out on a Hitachi S-4800 equipped with EDX at an accelerating voltage is about 10 kV. Sample preparation for FE-SEM visualization is slight and it comprises of arresting the materials on a double-sided carbon tape without further coating on it. The Powder XRD measurements are performed using a PANalytical X'Pert3 MRD diffractometer with monochromatized Cu Kα radiation (λ = 1.54 Å) at 30 mA and 40.0 kV. The measurement ranges for the samples (2θ) of 10–80° at a scan rate of 5° min^{-1} and a wavelength of 1.5405 Å. Raman spectra are measured on the XploRA Micro-Raman spectrophotometer (Horiba) with ranges is about 400.0–4000.0 cm^{-1}. Thermal analysis of the samples is analyzed with TA instruments and Universal V4.5 A Program is used to analyze the thermal curves. The accurate weight of each sample is 6.0 mg and the temperature range is 35.0–400.0 °C with a temperature hike is 10 °C/minute. XPS spectra are obtained using a K-Alpha

(Thermo Scientific). CasaXPS software is used for the deconvolution of the high-resolution XPS spectra. The carbon peaks are analyzed after the deconvolution of XPS data. The ^{1}H NMR and ROESY spectra of the ICs are done using an NMR spectrometer (Bruker 600 MHz). All the above instrument facilities are utilized at the core research support center for natural products and medical materials of Yeungnam University.

3. Results and discussion

3.1. Inclusion complexation of OTV with M-CD and S-CD

3.1.1. Phase solubility analysis

PS analysis has been performed to determine whether OTV solubility increases with a higher CD concentration [22]. Fig. 2 shows the phase solubility diagram based on the UV measurement results. In spite of the fact that OTV is soluble in water, we conducted the PS experiment to determine how soluble it is and to calculate the binding constant based on the interaction between them. As M-CD and S-CD concentrations increase, the OTV concentration rises linearly, suggesting the formation of a complex (OTV to CDs) with a 1:1 molar ratio. There have been previous studies showing that OTV and CD form a 1:1 complex [23,24]. According to our results, OTV has a water solubility of ~2.5 mM in the absence of both M-CD and S-CD, as well as an increase by ~1.5 and ~1.0 times at the highest concentrations of M-CD and S-CD. Based on the given experimental conditions, the binding constants (K_b) of OTV ICs are determined to be ~88.12 M^{-1} and ~95.68 M^{-1}, respectively. Phase solubility studies revealed that the slope is smaller than unity, over the entire concentration range studied, indicating an A_L-type diagram with the formation of inclusion complexes with 1:1 stoichiometry for both CDs. In addition, binding constants of the ICs are crucial components of their effectiveness because different effects derived from the formation of ICs are determined by their stability [25,26]. Low values of K_b indicate weak interactions and a high level of free CDs, whereas high values of K_b indicate that the equilibrium is shifted toward the formation of ICs. Ideal values are within the range of 100–1000 M^{-1} [27].

3.1.2. UV spectral analysis

In the presence of CDs, OTV absorbance changes which indicate complex formation and suggest OTV entering the cavity of the CDs [28]. OTV reaches its maximum at 217.0 nm in an aqueous medium (S. Fig. 1), indicating that the molecule is undergoing an n→σ * transition. In addition, the maximum in aqueous media has a shoulder-like shape and the transition is weak. After OTV molecules move from the polar aqueous environment into the apolar cavity of the CDs, there will be a change in the molar extinction coefficient (Δε) [29].

In this discussion, we can divide the UV changes for the OTV with CDs into two parts, since the spectral changes are completely different. In the first part, the concentration-dependent effect between OTV and M-CD is discussed. Adding M-CD gradually to OTV increases its absorbance without affecting the spectral maximum at 217.0 nm (S. Fig. 1**a**). No red or blue shift is observed at this wavelength. The second part concerns the concentration-dependent effect of OTV and S-CD. When S-CD is gradually added to OTV, we see a different pattern of absorption output. The OTV with S-CD exhibits two maxima at wavelengths of 217 nm and 250 nm (S. Fig. 1**b**). With S-CD, it is impossible to achieve two maxima. UV spectra have been measured for the S-CD without a guest molecule, OTV, in order to explain the unusual maxima. There are two maxima associated with the S-CD. Due to the formation of ICs, both spectral maxima are responsible for the S-CD and enhanced absorbance during its increased concentration in a host. The CDs will experience an increase in absorbance when they interact with small molecules, such as organic molecules or drug molecules [29], which primarily results in the formation of ICs. There are cases in which the spectral maximum does not shift.

In this case, it involves generating ICs between OTV and CDs by removing water from the cavity of the CD and by accommodating the OTV molecule, which contributes to the spontaneity of the process [30]. Hydrogen bonds, van der Waals interactions, and surface tension changes are also important. In this study, there appears to be some evidence that inclusion is usually concentration-dependent, with a guest molecule playing an important role [31]. An excess of CDs is used in this study (ca. 100:1, CD/OTV ratio) in order to maximize inclusion availability. A day after mixing OTV:CDs, we observe the final solution to be homogeneous and to contain ICs. The main way OTV interacts with the host's inner cavity is through hydrophobic contact (OTV does not have a polar characteristic). Among other factors, OTV:CDs-ICs adapt better to the cavity of the host than other CDs of similar size or shape, explaining the ease of incorporation [32].

Through the changes observed in UV measurement during the formation of ICs, it is possible to determine the binding constant (K_b), stoichiometric ratio, and Gibbs free energy changes (ΔG) [33]. Using the Benesi-Hildebrand equation [34], the double reciprocal plot (S. Fig. 2) has been drawn for 1:1 ICs [33,34]. K_b values are found to be 92.51 and 98.49 M^{-1} using the slope of the double reciprocal plots [33,35].

$$\frac{1}{\Delta A} = \frac{1}{\Delta\varepsilon.\ \ Kb.[OTV]} \times \frac{1}{[CDs]} + \frac{1}{\Delta\varepsilon.Kb}$$

In order to further understand the spontaneous nature of ICs, thermodynamic parameters can be used in order to describe the replacement of guest molecules within CDs and the subsequent exchange of water molecules during the formation of ICs. By measuring the Gibbs free energy change (ΔG) and the effect of temperature on the inclusion process, it can be determined if the inclusion process occurs spontaneously [29]. It is found that the ΔG for the ICs with M-CD and S-CD is − 6.235 and − 6.784 $kJ.mol^{-1}$, respectively, which provided information about the binding force between CDs and OTV [29] and that the nature of the reaction is exergonic and spontaneous.

Using the phase solubility method and the concentration-dependent method, it is possible to compare the K_b values of the ICs and assess the interaction between CDs and OTV. The results clearly show that OTV is stable in its hydrogen bonding interaction with secondary OH groups of CDs despite a small number of differences.

3.1.3. DRS analysis

S. Fig. 3 shows the diffuse reflectance spectra of ICs with respect to M-CD and S-CD. The OTV:M-CD-ICs are slightly more absorbent and slightly less reflective than ICs with S-CD in the UV region, due to interactions between the cavity CDs and OTV guests. The absorption and reflectance of both ICs are very similar, indicating a new binding between the guest and host.

3.1.4. FT-IR spectral analysis

FT-IR spectra provide great insight into the likely interactions between CD and guest molecules and therefore are a helpful tool for analyzing each guest molecule's functional groups as well as other characteristic peaks. Choi, Byeon, Park (2019) [36] suggest that the formation of ICs can shift or vary as a result of interactions with other molecules, indicating effective complexation. S. Fig. 4 summarizes the FT-IR spectra of OTV, M-CD, S-CD, and ICs with these components. In the pure OTV, there are stretching groups at 3500 cm^{-1} due to the N-H group. There are absorption bands at 1720 and 3342 cm^{-1} corresponding to C═O and N-H (secondary amine). The stretching groups of C-N, C═C (cyclic alkanes), and C-H (aliphatic) are also evident at 1200, 1610, and 2900 cm^{-1}, respectively. In the FT-IR spectrum of M-CD, the stretching O-H is at 3398 cm^{-1}; stretching C-H is at 2938 cm^{-1}; and stretching C-O- is at 1193, 1082, and 1022 cm^{-1}; (O-H stretching) is at 3398 cm^{-1}. ICs belonging to the secondary OH alcoholic group exhibit a wider peak, indicating the presence of CDs [37]. As with OTV and M-CD, the absorption bands have mostly shifted in the ICs, possibly as a result of vibrational restrictions induced by the complexation process. Additionally, a broader peak appears at 3400 cm^{-1} for O-H stretching, a weak band appears at 2901 cm^{-1} for C-H stretching, and a band at 1172 cm^{-1}

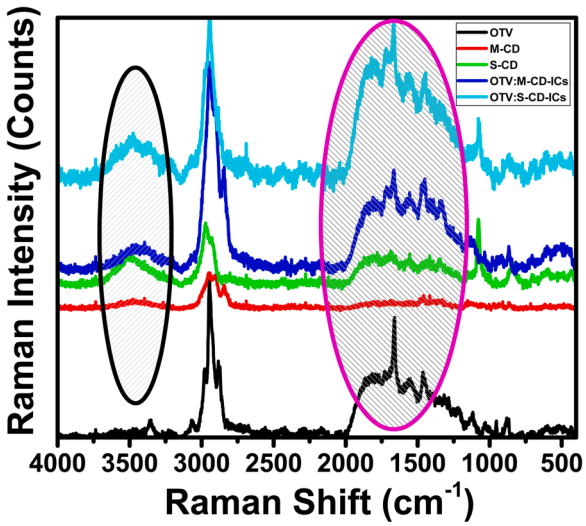

Fig. 3. Experimental Raman spectra of OTV, M-CD, S-CD, and their respective ICs.

belongs to C-O- stretching. Due to the effect of OTV, the broader peak of ICs with S-CD is almost reduced, and the peak intensity of OTV and S-CD is reduced to a maximum. A combination of OTV and CDs doesn't result in new chemical compounds, but the association of the two molecules by hydrogen bonding is evident in the large shift in peak position for both the ICs over the free materials OTV, M-CD, and S-CD, demonstrating how the cavity in the host affects the guest molecule, resulting in the formation of a complex [38]. The existence of ICs between OTVs and CDs is plausible. Based on IR, there may be different interpretations of the inclusion of OTV with CDs. The C═O group frequency changes for both ICs, indicating that the OTV may also exist within the cavity of CDs. OTV with CDs exhibits no variations in stretching frequencies in other parts of the guest molecule, which suggests that these parts might not be contained within CD cavities.

3.1.5. Raman spectral analysis

It is demonstrated by Raman spectroscopy that the IC formed by curcumin and derivative cyclodextrins is distinct and clear [39]. Earlier studies have used Raman spectroscopy to characterize the ICs [40]. ICs with M-CD and S-CD in the solid-state have not yet been characterized using Raman spectroscopy. As shown in Fig. 3, Raman spectroscopy is used to determine the OTV content in ICs, and the spectra of OTV, M-CD, and S-CD are displayed as well as their respective ICs. The experimental spectra of the OTV, M-CD, S-CD, and ICs have five main Raman bands. All have been assigned to the following categories: γ (CH3), γ (C═O), γ (N-H), γ (O-H), and γ (C-O-C). With respect to the stretching groups cited above, peaks are observed at 2950, 1700, 3200, 3450, and 1130 cm^{-1}. Since OTV doesn't have a broad peak at 3400 cm^{-1}, it doesn't contain any OH groups. CDs in ICs show a broader peak at 3425 cm^{-1}, suggesting the presence of the OH group. There is also no C═O peak in either CD. As well as the OTVs, the CDs are also found in ICs, revealing that these products (ICs) have both the OTVs and the CDs. It is possible that the peak for the main groups of OTV has shifted during the formation of the ICs with CDs. Although the Raman spectra of the two ICs appear similar,

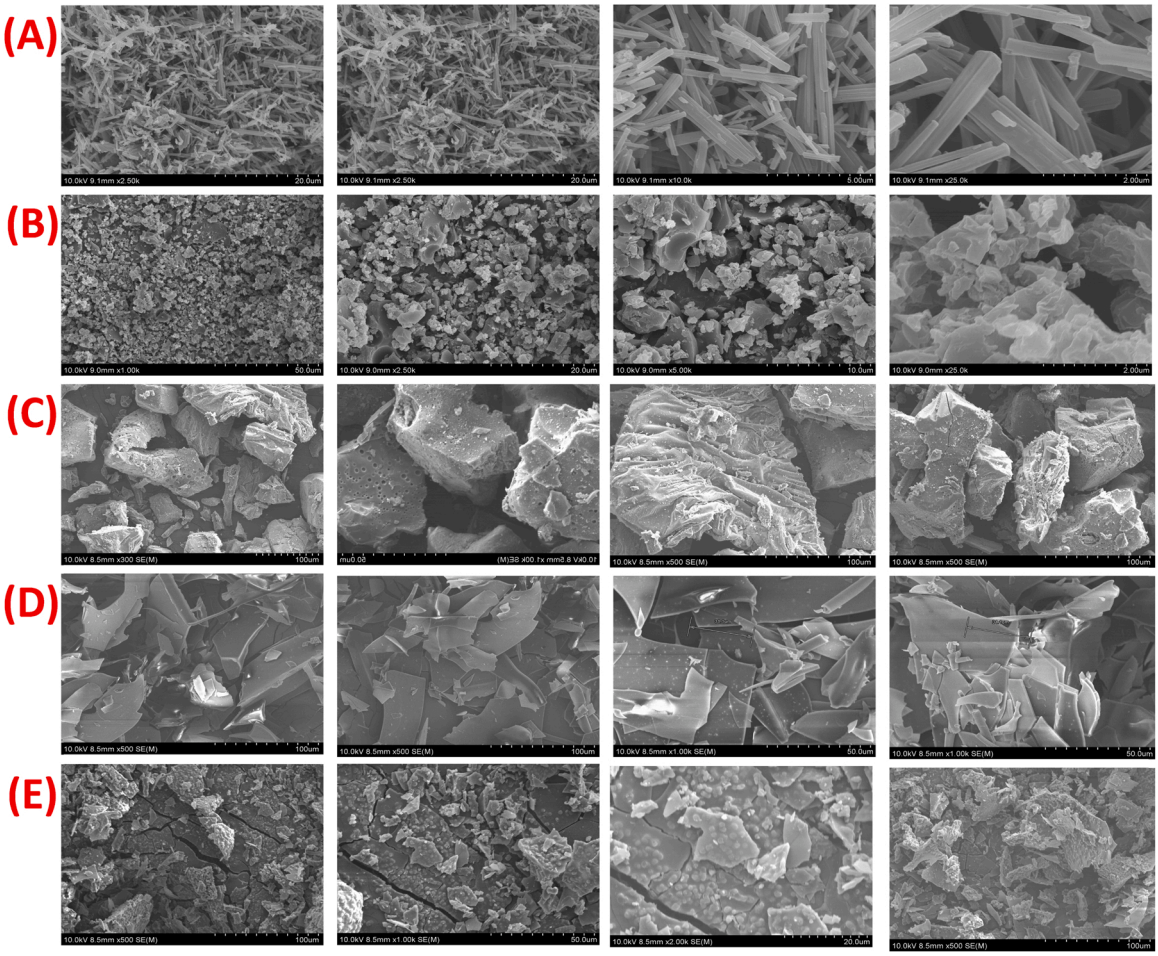

Fig. 4. The visual representative SEM images of (A) OTV, (B) M-CD, (C) S-CD, and their respective ICs (D & E).

the OTV content in the two ICs is vastly different. Based on the Raman spectra, it appears that the CD efficiency of ICs can be rated as follows: OTV:M-CD-ICs < OTV:S-CD-ICs.

3.1.6. XRD analysis

XRD analysis is used to examine the formation of ICs in more detail. Therefore, it may be a convenient way to confirm ICs in that the amorphization of the guest molecules can be altered by the disappearance or shift of their sharp peaks [41,42]. S. Fig. 5 illustrates the XRD patterns for OTVs, CDs, and ICs. OTV and M-CD show characteristic diffraction peaks at different diffraction angles (2θ). There is a clear crystal peak of OTV at 11.45, 13.87, 15.91, 19.54, 24.67, and 26.86. XRD patterns of M-CD reveal two broad peaks at 11.5 and 22.3. Likewise, the S-CD is also amorphous, as shown by the XRD pattern, which revealed a broad peak at 24.4. Those broad peaks reflect the amorphous nature of those materials. As a result, M-CD, as well as S-CD in powder form, do not show any other characteristic diffraction peaks. The diffraction peaks observed in CDs are only around 10° and 20°, which indicates an amorphous state [43]. Thus, after making ICs, the relative content of OTV reduces the intensity of the characteristic diffraction peaks. Based on the pattern of the ICs, amorphous materials lose their crystallinity when they undergo complexation, indicating that the OTV has been encapsulated in the cavity of the CDs [44,45]. This revealed the OTV molecule is completely amorphized after stable hydrophobic interactions with both the CDs [46,47].

3.1.7. AFM analysis

AFM scans the samples with a nanoscale probe to produce detailed topographic images. Therefore, AFM can be used to observe nanometer-scale surface roughness and texture even when the surface features are smaller than 3 μm in size [48,49]. There is a slight aggregation after 2D and 3D images based on OTV, M-CD, and S-CD (S. Fig. 6). Both ICs had the same surface morphologies compared with guests, OTV, because the particles are randomly placed in the field of vision. On the other hand, the OTV is characterized by large aggregates with square crystal shapes. There is strong evidence for changes in surface topography and crystal structure of the ICs over time [50,51]. In contrast to the free molecules of guests and hosts, the ICs have a lower surface roughness. Incorporating OTV into the cavity of CDs provides an additional level of confirmation.

3.1.8. FE-SEM morphological analysis

The surface morphology of samples such as OTVs, M-CDs, S-CDs, and ICs is usually visualized by FE-SEM [41,42]. Fig. 4 depicts SEM images of the OTV and the respective ICs formed with CDs. As a result of its crystallinity, the OTV sample displays clear, needle-like crystalline structures with smooth surface. As compared to OTV, M-CD and S-CD showed small and large rock-like structures throughout the sample. ICs and OTVs of the formed complex have different morphologies. All magnifications revealed a different structure for the lyophilized product of ICs. The free materials of OTV and CDs do not resemble each other when it comes to morphological visualization. Therefore, the OTV and raw CD materials are completely merged in the ICs to produce a new morphological surface. Furthermore, EDX output clearly shows the presence of C, O, P, S, and Na in the ICs at the appropriate percentage (S. Fig. 7). There is nothing in either of the CDs that contain P, S, or Na. The information is only shown in the ICs, suggesting an interaction between the OTV and CDs. Inclusion interactions are evidenced by the atomic percentages of C, O, P, and S, as well as Na in ICs. ICs are characterized by morphological differences and elemental presence, which provide the strongest evidence that they formed.

3.1.9. TGDTA curve analysis

A thermogravimetric analysis (TGA) combined with gradual and continuous temperature increases is among the simplest and most common methods of studying the thermal behavior of ICs. The thermal behavior of ICs is studied using TGA/DTA as a function of temperature. Various methods are used to calculate E_a values [52,53].

A change in weight caused by decomposition, oxidation, or any other physical or chemical process can be measured simultaneously. In addition, TGA and DTA are used to analyze the ICs. The TG and derivative curves of OTV, along with the ICs are shown in S. Fig. 8. A two-stage weight loss process has the greatest effect on OTV and ICs. Up to 195.0 °C, the OTV molecule performs well and its weight does not significantly change. Weight loss begins at 193.0 °C and continues until 294.4 °C. Approximately half of the weight loss occurs between 193.0 and 294.4 °C. TGA curves for CDs can be viewed as both a result of evaporation and phase transitions [54,55]. There are two stages to weight loss for ICs. There is a slight decrease in weight loss owing to dehydration of the ICs up to a temperature of 100 °C. As for the second one, not as small loss refers to the weight loss that occurs after 244.0 °C and 235.0 °C for ICs with M-CD and S-CD, respectively, and the weight loss continues up to 266.6 and 254.6 °C with no further weight loss. This duration of time has led to approximately 55% of weight loss, which may be due to the temperature associated with both OTV and CD decomposition. It has been shown that the thermal behavior of OTV can be significantly changed by making ICs with hosts like M-CD and S-CD [56]. As a result of OTV inclusion in CD cavities, there is a change in decomposition temperature, indicating that the thermal stability of the OTV:M-CD-ICs has been improved. An important change in the inclusion process could be evident as well.

The DTA analysis defines whether decomposition takes place endothermically or exothermically. In addition, the DTA analysis revealed the presence of OTV within the cavity of CDs (S. Fig. 8). As expected from their chemical structure and physical characteristics, natural and modified CDs (methylated and sulfated) have similar thermal behavior [56,57]. Mass loss and water content are clearly different quantities [56]. OTV produced a sharp peak at 194 °C and a more rounded peak at 268 °C during this period, indicating the hydrogen bonding process releases heat. In both cases, there is only a single significant peak at the temperatures of 248.4 °C and 264.2 °C for the ICs with M-CD and S-CD, respectively, and there are no broader peaks at those temperatures.

3.1.10. NMR analysis

A new mode of assigning proton signals to OTV, M-CD, S-CD, and ICs is developed in DMSO at room temperature based on the ^{1}H NMR spectrum. The assignment of CDs is based on the literature [58–60]. The ^{1}H NMR spectra of both CDs and the OTV molecule reveal chemical shift changes after OTV is incorporated into the CDs cavity.

3.1.10.1. ^{1}H NMR analysis of OTV:M-CD-ICs. In the ^{1}H NMR spectrum of OTV, as expected two triplets and multiplets are observed in the more shielded region at 0.78, 0.83, and 1.41 ppm. The signals are conveniently assigned to ethyl groups attached to ether linkage at C-3. A triplet and a multiplet observed at 1.22 and 4.15 ppm with an equal splitting space are assigned to the carbethoxy ethyl group at C-1. A sharp singlet observed at 6.64 ppm is assigned conveniently to the methine proton at C-2. Protons with an electronegative environment (attached with nitrogen and oxygen) are observed in the range of 3.13–4.15 ppm (S. Fig. 9). The multiplets observed at 2.20 and 2.72 ppm are due to ring protons. The individual assignment is done by analyzing the ROESY spectrum of the ICs. The ^{1}H NMR spectrum of M-CD shows multiplets at 5.54–5.88 ppm and 4.44–5.03 due to axial protons of the M-CD ring, other methine protons of methylated cyclodextrin ring, and methylene protons are observed in the range of 3.22–3.74 ppm (S. Fig. 9). Methoxy protons appear as singlets at 3.61 ppm.

In the ^{1}H NMR spectrum of ICs, most of the proton signals are shifted to the shielding region by 0.01–0.32 ppm. In this, the amide NH proton signals at C-4 in the complex are shifted by 0.36 ppm and it is observed at 7.88 ppm (S. Fig. 9). The methyl protons of the amide group are also shifted to unfield by 0.02 ppm and it is observed at 1.86 ppm. The proton signals of H-6a and H-5a observed at 2.20 ppm and 2.72 ppm in

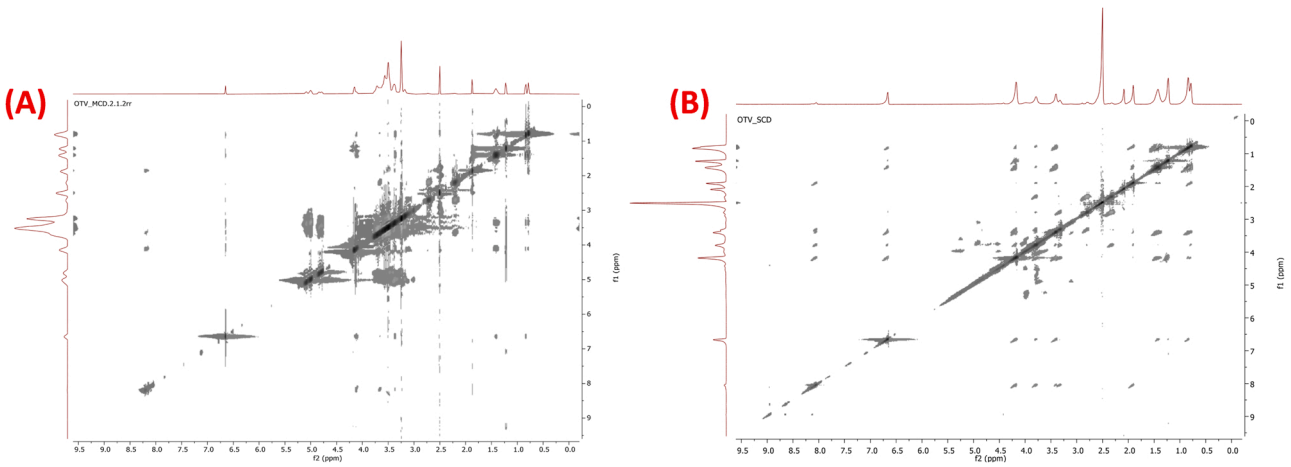

Fig. 5. ROESY Spectra of (A) OTV;M-CD-ICs and (B) OTV:S-CD-ICs.

the OTV are deshielded by 0.1 ppm and these protons are observed at 2.10 and 2.82 ppm in the complex. All the other protons are shifted by 0.01–0.02 ppm and these are negligible. Interpreting the proton signals of the complex, in the proton NMR spectrum both M-CD and OTV signals are present. When comparing the signals of M-CD with complex, multiplet at 5.54–5.88 ppm is shifted to shielding region by 1 ppm and the signal is getting broadened and due t appeared like a hump. Here the above signal is due to the axial proton of the M-CD. In the proton NMR spectrum of the ICs, most of the protons have appeared in the region of 3.17–4.17 ppm. the individual assignments OTV, M-CD, and its ICs are done with the help of the ROESY spectrum.

3.1.10.2. Analysis of OTV:M-CD-ICs by ROESY. In the ROESY spectrum, the correlation is observed between signals at 6.64 with signals at 0.80, 0.84, 1.41, 3.36 and 4.15 ppm. Among the above correlation proton signals 0.80, 0.84 and 1.41 are already assigned to the ethyl group of the ether linkage at C-3 (Fig. 5A). Hence the remaining two signals at 3.36 and 4.15 ppm are due to the methine proton of the ether and H-3a proton. A doublet at 2.10 ppm is assigned to the axial proton of the methylene group at C-6. It has a strong correlation with 2.72, 4.15, and 3.66 ppm. Hence 2.72 may be due to H-5a and 3.66 ppm is due to another methylene proton at C-6. The proton signal at 4.15 is due to the methylene proton of the ethoxy carbonyl group at C-1. And the remaining signal at 3.13 is conveniently assigned to H-4a. With the help of all the above correlations, individual assignments of the proton signals are done without ambiguity for OTV, M-CD, and its ICs. The proton chemical shift of OTV is presented in S. Table 1.

In addition to the correlations obtained already few more important correlations are in the ROESY spectrum helped us to confirm the formation of the ICs. A correlation is obtained between the methoxy group

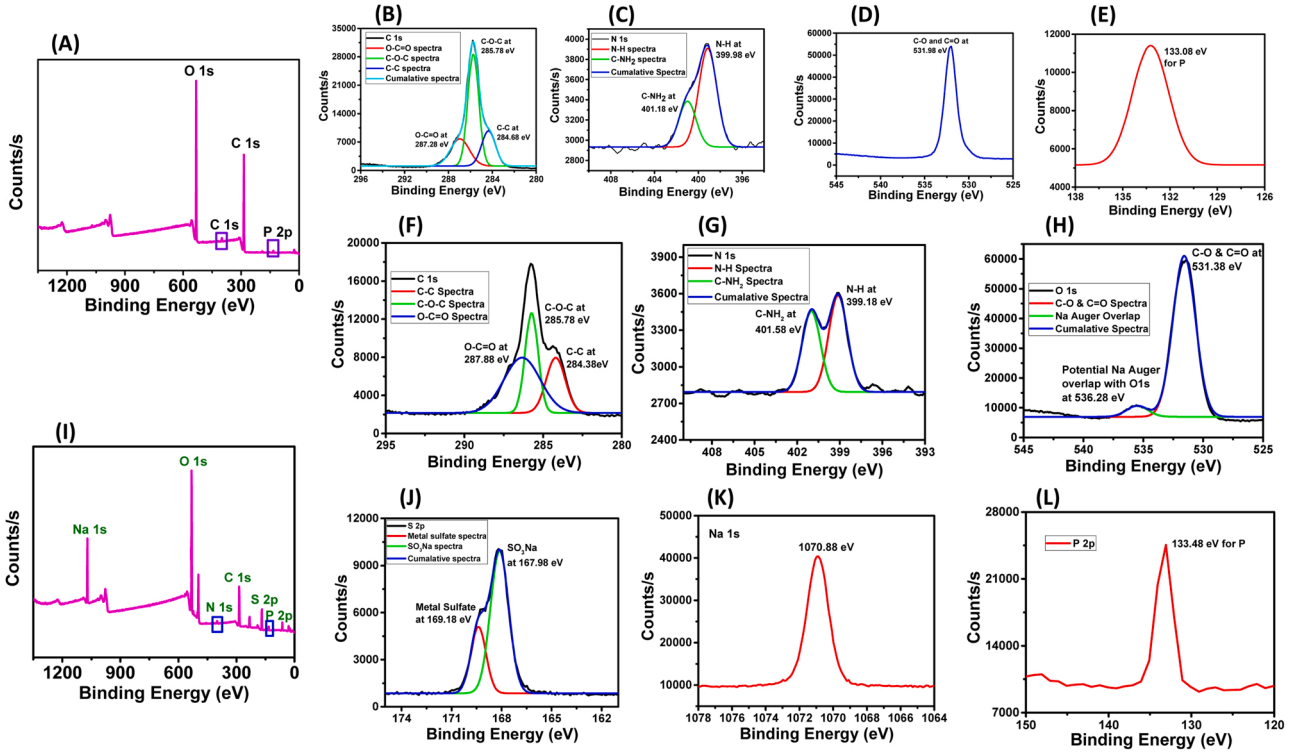

Fig. 6. XPS survey spectra for ICs with M-CD and S-CD (**A**) & (**I**). XPS high-resolution spectra of (**B**) & (**F**) C 1 s, (**C**) & (**G**) N 1 s, (**D**) & (**H**) O 1 s, (**E**) & (**L**) P 2p, (**J**) S 2p, and (**K**) Na.

Table 1
Energies for the ICs with M-CD and S-CD.

Parameters	OTV	M-CD	S-CD	OTV:M-CD-ICs		OTV:S-CD-ICs	
				Orientation A	Orientation B	Orientation A	Orientation B
E (eV)	-5219.95	-21488.73	-23614.16	-26709.98	-26709.98	-28836.81	-28833.18
E_{HOMO} (eV)	-9.931	-9.236	-10.130	-9.732	-9.597	-10.100	-9.188
E_{LUMO} (eV)	-0.957	-0.415	-0.095	-0.874	-0.912	-0.532	-0.750
Δ (E_{HOMO}-E_{LUMO}) k.cal.mol^{-1}	-8.974	-8.821	-10.035	-8.858	-8.685	-9.568	-8.438

of M-CD at 3.57 ppm with 0.80, 0.84,1.86, 2.82, 4.15, 4.84–5.02, 6.64 and amide proton of OTV at 7.88 ppm. Among the correlations, the proton signals at 0.80, 0.84, 1.86, 2.82, 4.15, 6.64 and 7.88 ppm are due to protons of OTV. The remaining signal is due to the M-CD protons. It is further confirmed by proton signal due to H-3a of OTV at 4.15 ppm showing correlations with 0.80, 0.84, 1.22, 1.41, 2.82, 4.91, 6.64and 7.88 ppm. From the above signals 0.80, 0.84, 1.22, 1.41, 2,82, 6,64 and, 7.88 are already assigned to the ethyl group of the ether linkage at C-3 and the ester group at C-1, H2a and amide proton at C-5 of OTV. H-3a has a correlation with 4.94 ppm of M-CD. The signal at 4.94 ppm is due to the axial proton of methylated cyclodextrin. An important correlation is obtained between amide protons at 7.88 ppm with methyl protons at 1.86, H-3a (4.15) and M-CD protons at 3.50 ppm. Hence the correlation obtained from the ROESY spectrum confirms there is an interaction between M-CD with OTV. The above discussion reveals that the structure of the compound may be proposed as follows (S. Fig. 10).

3.1.10.3. ^{1}H NMR analysis of OTV:S-CD-ICs. In the ^{1}H NMR spectrum of S-CD shows multiplets at 5.09–5.4.79 ppm and 4.54 are due to axial protons of S-CD ring, other methine protons of S-CD ring and methylene protons are observed in the range of 3.22–3.74 ppm and 4.16 ppm (S. Fig. 9). The ^{1}H NMR spectrum of the above ICs shows proton chemical shifts due to OTV observed at 8.02, 6.65, 4.16, 3.59, 3.36, 3.13, 2.20, 2.72, 1.42, 1.23, 0.77 and 0.83 ppm. All other signals are due to another partner. In the ^{1}H NMR spectrum of S-CD the chemical shifts observed at 5.09–5.4.79 ppm and 4.54, 4.16 ppm are assigned to the axial proton of the S-CD ring. In the above signal, most of the signals are shifted towards the shielding region by 1 ppm. The individual assignments are done by analyzing the ROESY spectrum.

3.1.10.4. Analysis of OTV:S-CD-ICs by ROESY. In the ROESY spectrum, the correlation is obtained between the methyl proton at 0.78 ppm and the signals at 1.22, 1.86, 3.36, 3.66, 4.15 and 6.64 ppm (these signals are due to OTV). And these signals are already assigned to methylene,

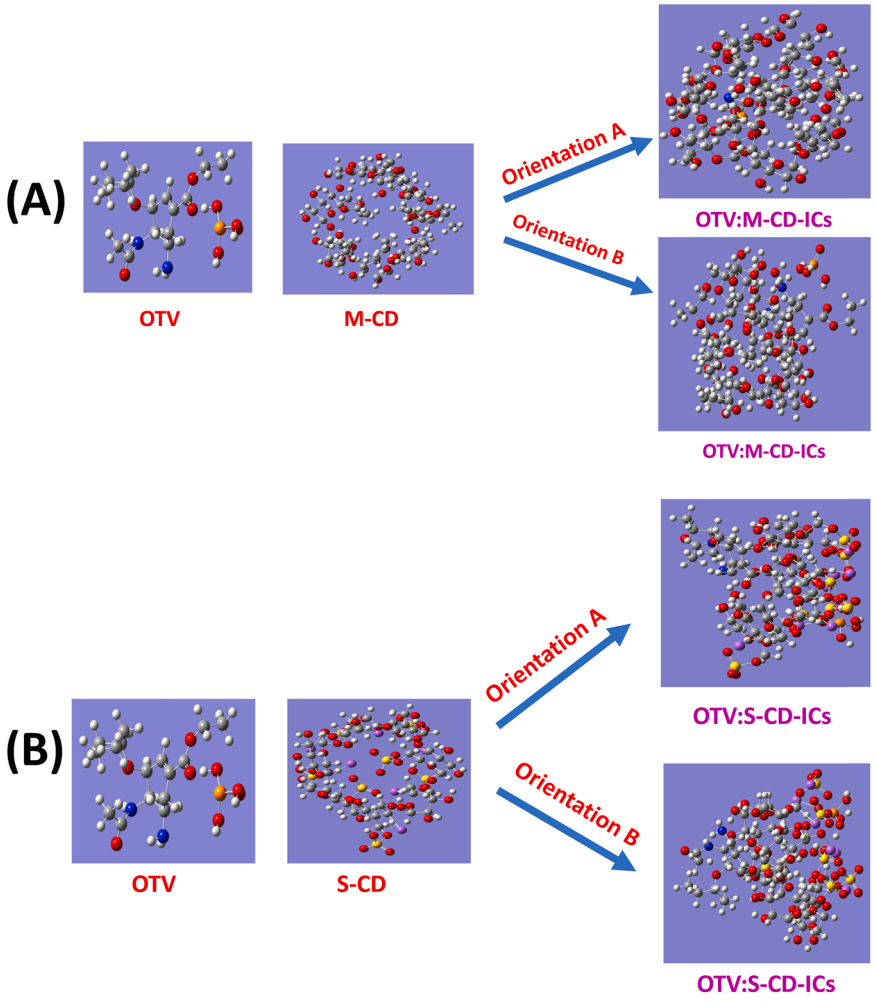

Fig. 7. Possible orientations of (A) OTV:M-CD-ICs and, (B) OTV:S-CD-ICs.

and methine of the ether linkage at C-3, H-3a, H-4a, H-2a and H6e of the OTV component (Fig. 5B). In the ICs, the proton at 4.16 ppm of SCD moiety is shifted to 3.99pmm in the complex, which has a correlation with 3.66, 4.54 and 5.10 ppm. Among the above three correlations, the signals at 4.54 and 5.10 ppm are due to the methylene and axial protons of the S-CD moiety. The remaining signal is due to the H-6e proton of the OTV moiety. Since this correlation is very much useful for the confirmation of inclusion complex formation. Further, the formation of the ICs is confirmed by another correlation, i.e proton chemical shift at 3.71 ppm which is due to the methine proton of the SCD moiety having correlations with 0.80, 1.41, 1.86, 2.20,2.72, 3.13, 4.15,4.54, 4.72, 6.64 and 8.01 ppm. Among the above relations the proton chemical shifts at 0.80, and 1.41 are already assigned to the methyl and methine of the ether part. Methine proton of SCD also has a correlation with 2.20,2.72, 3.13, 4.15, and 6.64 due to H-2a, H-3a, H-4a, and H-5a protons of OTV moiety. Also, it shows strong binding with amide NH proton and its methyl substituent. All other signals 4.54 and 4.72 ppm are due to methine protons of the S-CD moiety. This correlation confirms the formation of the ICs and it reveals that the structure of the ICs has been presented in S. Fig. 10.

3.1.11. XPS analysis

XPS surface analysis is most commonly used for chemical analysis since it is applicable to a wide variety of materials and provides valuable information about the materials and their chemical state, as well as their chemical composition. We have used XPS as well as elemental compositions of C, O, N, P, S, and Na to determine whether OTV and CDs have interacted on the surface of ICs. There is great importance in this physical evidence for an IC's chemical composition. As shown in Fig. 6, ICs are exposed to a wide energy survey spectrum. The XPS measurement can be used to find C, O, N, P, S, and Na in ICs. Both C and O contribute to CDs and OTVs. N and P are also present in OTV. C, O, N, and P are found on the surfaces of ICs when they are formed.

M-CD and S-CD samples do not contain N or P, except for carbon and oxygen (please refer to individual element analysis for details). Consequently, oxygen and phosphorus can provide evidence of OTV surface content on ICs. Interestingly, the data indicate that individual elements exist in ICs. Furthermore, S-CD ICs consist of S and Na, as the sulfated sodium salt of CD exists. When the binding energies of particular elements are compared to the spectral outputs, it is revealed that the host cavity is about the same surface area to encapsulate an OTV. For the first element C, it consists of C-C, C-O-C, and O-C═O, for the second element O it is C-O, for the third element N it consists of C-NH_2, N-H, and for the fourth element P, it consists of P-OH. It appears that the binding energies of C, O, N, and P for both ICs and their respective binding energies are similar. The synthesized ICs are also confirmed as being of the highest purity because they appear to peak as per the established reference in the literature and provided in S. Table 2. As shown by the tabulated energy values and the survey spectrum, a stable and true complex has been formed. As a piece of secondary evidence, atomic percentages are also used to support ICs.

3.2. Orientations of ICs by DFT calculations

Table 1 shows the combined complexation energy (E) for both the A and B orientations of the ICs. As shown in Fig. 7, both ICs can be oriented in various ways. According to Table 1, the complexation energies in a vacuum for both the ICs, orientation A is stable. In terms of the PM3 calculations, the differences between the models are about the same as those between the ICs. On the other hand, the energy suggests that the other orientations are the least likely. ICs with decreasing complexation energies are generally regarded as having the most advantageous orientation. Therefore, ICs with an A orientation for both ICs are considered to be more stable than those with the other orientations.

The two most important parameters in quantum chemistry are HOMO and LUMO. As with drugs, compounds with large HOMO-LUMO values tend to be more stable since they are associated with a large gap Δ (E_{HOMO} - E_{LUMO}). In both ICs, the A orientation is projected to have a higher energy gap than the B orientation. These results suggest that the A orientation is more reliable and advantageous for ICs with CDs compared to the B orientation.

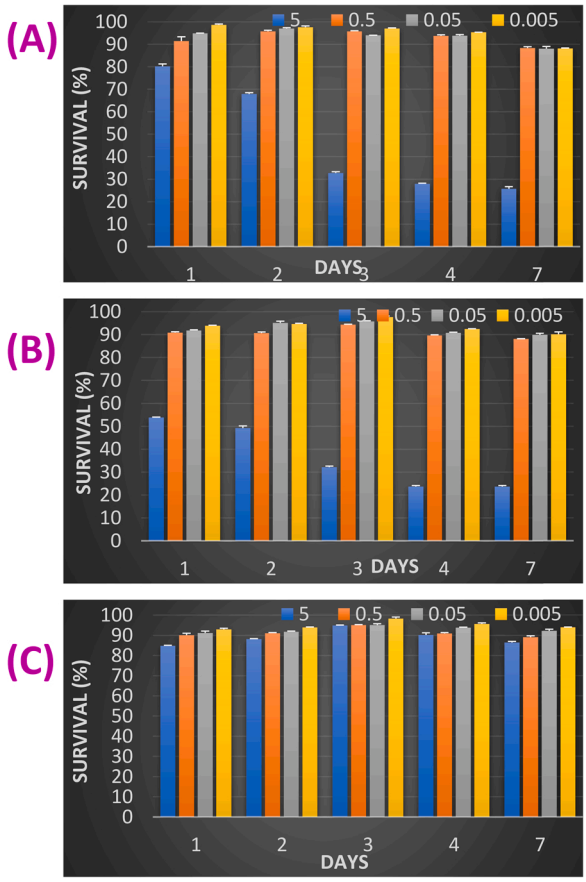

Fig. 8. Cell viability with (A) OTV, (B) OTV:M-CD-ICs and (C) OTV:S-CD-ICs on MRC-5 cell by the Alamar blue assay.

One of the most significant properties of CDs is that their ability to complex is a ward with dipole second. Due to the altered extremity of CDs, the dipole second is responsible for balancing out the framed ICs. In Fig. 7, the variety of dipole moments for the respective ICs is shown for M-CD (5.98 and 5.74 Debye) and S-CD (5.39 and 5.99 Debye). Thus, the polarity of ICs determines their dipole moment. Self-assembly and ICs are largely driven by hydrogen bonds via hydrophilic and hydrophobic interactions, as shown in a simulation study [61,62]. Due to our consideration of energy as the primary concern, we identified the most stable complex in the ICs with A orientation.

3.3. Drug release analysis

Semipermeable membranes are used in the gastrointestinal barrier, which prevents ICs from passing and semipermeable membranes allow only OTVs or CDs to pass. In the presence of CDs, OTV absorption will be slower due to rapid IC formation. In general, water-soluble drugs are chosen to demonstrate that even after complete dissolution, ICs can form with CDs. These complexes are water-soluble, but they may slow down the absorption of drugs such as OTV, since the rate at which the drugs dissociate from the CDs could be the speed limiting factor. As the drug is released through gastric transit within eight hours after dissociation, this becomes extremely relevant. The example presented here highlights the importance of a thorough examination of the potential OTV:CDs-ICs, which can be used as a screening step during formulation

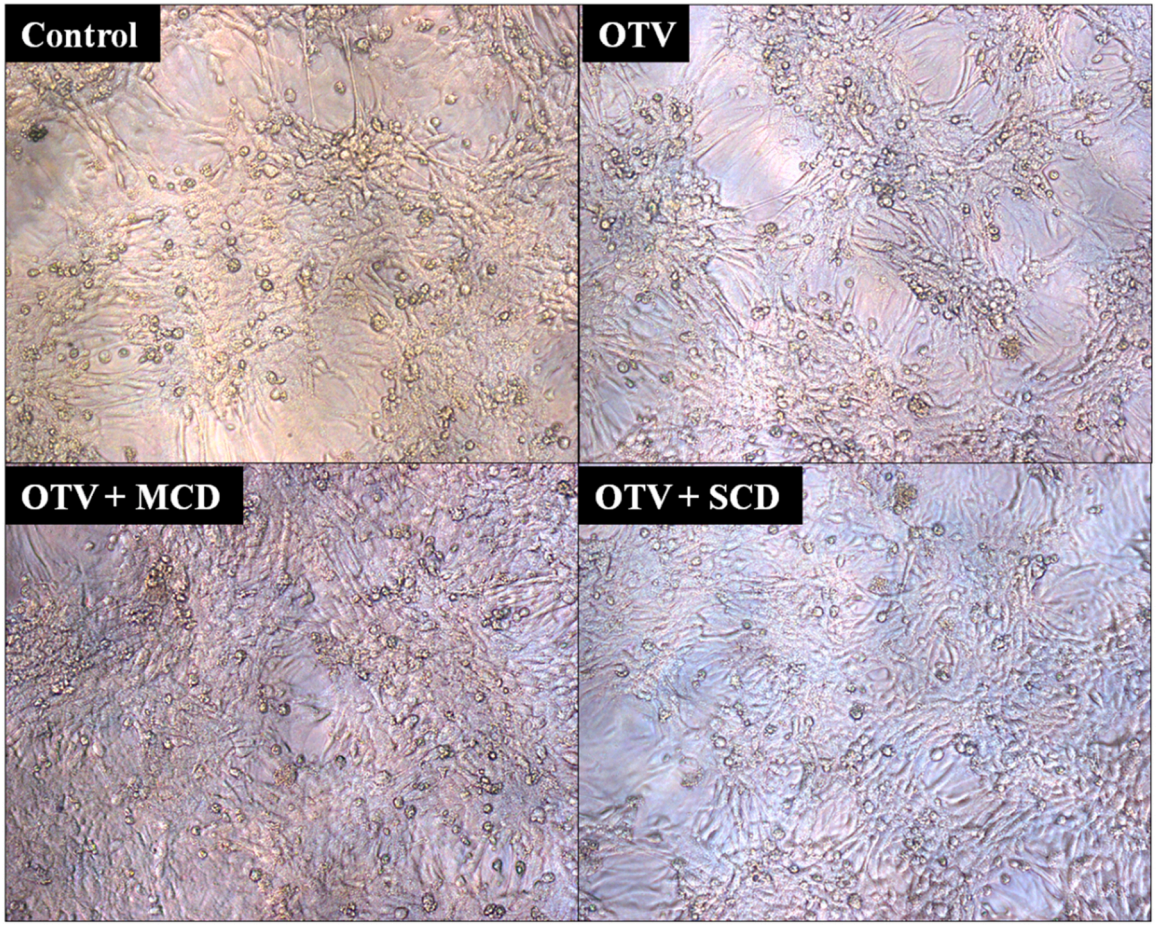

Fig. 9. Brightfield images of OTV and ICs treated on MRC-5 cells.

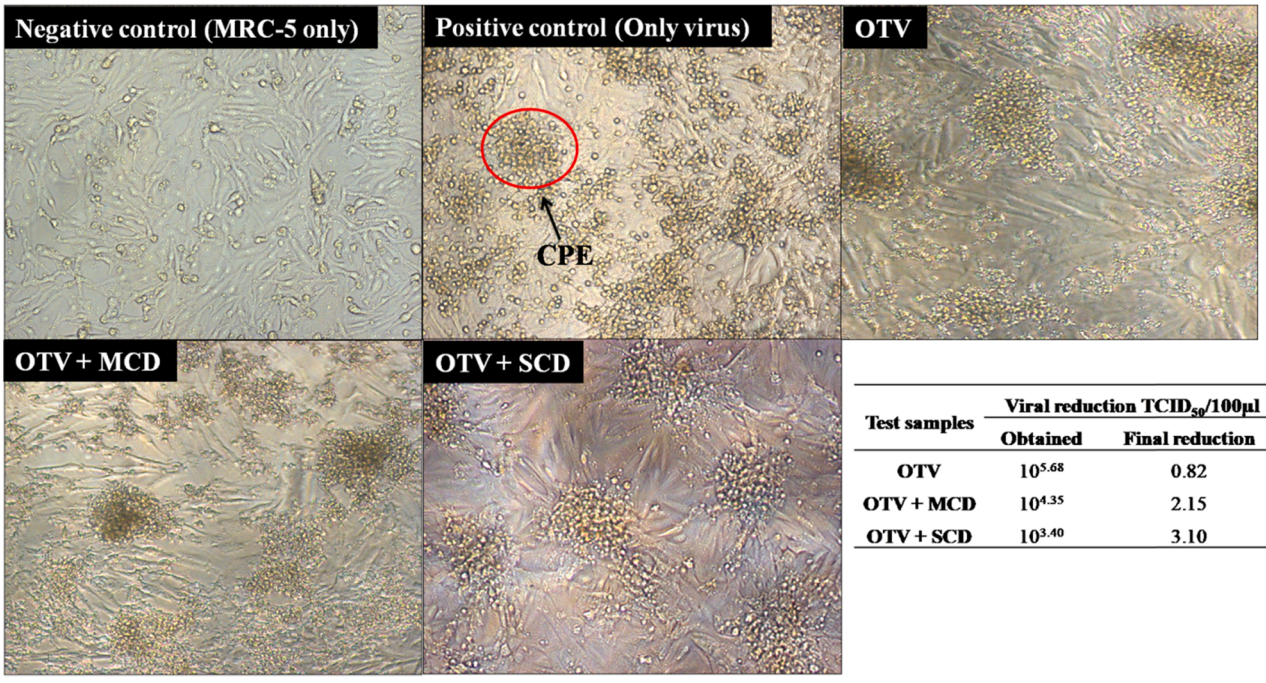

Test samples	Viral reduction $TCID_{50}$/100µl	
	Obtained	Final reduction
OTV	$10^{5.68}$	0.82
OTV + MCD	$10^{4.35}$	2.15
OTV + SCD	$10^{3.40}$	3.10

Fig. 10. Brightfield images of OTV and ICs with HCoV-229E infectivity in MRC-5 cells.

development or before formulation development.

According to the analysis of drug release experiments conducted in three different pH phosphate buffers, the formulation releases significant amounts of drugs in both ICs. The maximum drug release of OTV in ICs is found to occur at 7 h for three different pH levels. The OTV:S-CD-ICs showed essentially 98% release in 7 h on pH 6.8 and pH 5.2, but the OTV:H-CD-ICs exhibited only 78% release. When the pH level is lower than pH 7.3, the drug-releasing behavior has reached a maximum. When the condition is not acidic, the OTV trend is almost the same as with M-CD. Release profiles typically take longer to complete depending on the direction and mode of binding [63–65]. S-CD ICs will exhibit greater cytotoxicity and viral inactivation because of their releasing profile. The *in-vitro* drug release profiles are shown in S. Fig. 11 together with the standard deviations for both ICs.

3.3.1. *Cell viability*

We used the Alamar blue cytotoxicity assay to determine the degree of damage caused by ICs like OTV:M-CD-ICs and OTV:S-CD-ICs on the MRC-5 cell line (Fig. 8). According to OTV results, cytotoxicity increased as the concentration increased (0.005–5.0 mg/ml), 80.2% of cells survived after 1 day and 25.7% survived after 7 days at 5 mg/ml, and other concentrations showed much less toxicity. In the assay performed for ICs, 5 mg/ml caused a toxic effect on the MRC-5 cells, but other concentrations caused little damage (less than 20%), and Fig. 9 shows a 10X view of ICs in 0.5 mg/ml. CDs are the perfect carrier host molecules in terms of improving solubility, low toxicity and versatility to accommodate diverse chemical modifications [66].

3.3.2. *Cytopathic effect ($TCID_{50}$)*

A comparative analysis of the antiviral activity (alpha human coronavirus 229E) of the three samples (OTV, ICs with M-CD, and S-CD) revealed that OTV:S-CD-ICs had the highest antiviral activity, they reduced 3.10 Log $TCID_{50}$/100 µl and others are less reduce by 2.15 for OTV:M-CD-ICs and 0.81 by OTV. On the day of 4th day started the cytopathic effect on the surface of cells, all the derivatives 10^{0} to 10^{-2} dilutions had 100 % CPE within 5 days ICs with SCD have less CPE (Fig. 10). Modified CDs are used to increase their antiviral activities after making the drug OTV as ICs. It may be due to the much better binding interaction with S-CD over the M-CD.

4. Conclusions

A successful sonication method has been developed for the formation of ICs, and they have been characterized adequately with analytical techniques. Analyses of elemental composition have been carried out by means of EDAX and XPS, which confirm the presence of OTV and CD in the ICs. ^{1}H NMR and ROESY results confirm the formation of ICs and the cyclic part of the OTV molecule has involved the interaction and other parts lie outside of the cavity of CDs. It is interesting to note that ICs with CDs are formed within the cyclic cavity of CDs and part of the OTV is included in the cavity. There is no conflict with the interpretation of IR and NMR results for both orientations that confirm ICs. ICs made after using both CDs have considerably changed their roughness and morphology. The slow release of OTV from the ICs found through drug release analysis and helps to contribute towards the virus inactivation. The formation of syncytium in both the ICs is decreased with the addition of MRC-5 cells, indicating that better inactivation is achieved and it is the first report of the virus inactivation with the help of water-soluble ICs. OTV:S-CD-ICs displayed lower CPE than OTV:M-CD-ICs and it would result in improved performance for the ICs. Hence, this research has succeeded in its intended purpose.

CRediT authorship contribution statement

Rajaram Rajamohan: Conceptualization, Methodology, Interpretation, Writing – original draft. **Sekar Ashokkumar:** Methodology, Writing – original draft. **Kuppusamy Murugavel:** Interpretation, Writing – original draft. **Madi Fatiha & Neour Leila:** Methodology. **Sonaimuthu Mohandoss**: Funding acquisition **Yong Rok Lee**: Review & editing, and supervision.

Declaration of Competing Interest

There are no conflicts of interest to declare.

Data availability

The data that has been used is confidential.

Acknowledgments

We are grateful for the support from the National Research Foundation of Korea (NRF) grant funded by the Korean government (MSIT) (2021R1A2B5B02002436).

Appendix A. Supporting information

Supplementary data associated with this article can be found in the online version at doi:10.1016/j.jpba.2022.115057.

References

[1] S.B. Carneiro, C. Duarte, F. Ílary, L. Heimfarth, S. Quintans, J. De Souza, J., L. J. Quintans-Júnior, V.F. Veiga Júnior, Á.A. Neves de Lima, Cyclodextrin–drug inclusion complexes: in vivo and in vitro approaches, Int. J. Mol. Sci. 20 (2019) 642–648.
[2] P. Saokham, C. Muankaew, P. Jansook, T. Loftsson, Solubility of cyclodextrins and drug/cyclodextrin complexes, Molecules 23 (2018) 1161.
[3] T. Loftsson, P. Saokham, A.R. Sá Couto, Self-association of cyclodextrins and cyclodextrin complexes in aqueous solutions, Int. J. Pharm. 560 (2019) 228–234.
[4] P. Jansook, N. Ogawa, T. Loftsson, Cyclodextrins: structure, physicochemical properties and pharmaceutical applications, Int. J. Pharm. 535 (2018) 272–284.
[5] M. Messner, S.V. Kurkov, M.E. Brewster, P. Jansook, T. Loftsson, Self-assembly of cyclodextrin complexes: aggregation of hydrocortisone/cyclodextrin complexes, Int. J. Pharm. 407 (2011) 174–183.
[6] G. Utzeri, P.M.C. Matias, D. Murtinho, A.J.M. Valente, Cyclodextrin-based nanosponges: overview and opportunities, Front. Chem. 10 (2022), 859406.
[7] P.M. Maheriya, Cyclodextrin: a promising candidate in enhancing oral bioavailability of poorly water-soluble drugs, Moj. Bioequiv. Availab. 3 (2017) 60–63.
[8] S. Karim Shalaby, M.I. Ismail, A.L.F. Lamprecht, Cyclodextrin complex formation with water-soluble drugs: conclusions from isothermal titration calorimetry and molecular modeling, AAPS Pharm. Sci. Tech. 7 (2021) 232.
[9] I.M.V. Enoch, M. Swaminathan, Dual fluorescence and photoprototropic characteristics of 2-aminodiphenylsulphone-β-cyclodextrin inclusion complex, J. Incl. Phenom. Macrocycl. Chem. 53 (2005) 149–154.
[10] S.B. Carneiro, F.I.C. Duarte, L. Heimfarth, J.D.S.S. Quintans, L.J. Quintans-Júnior, V.F.D.V. Júnior, A.A.N. De Lima, Cyclodextrin-drug inclusion complexes: in vivo and in vitro approaches, Int. J. Mol. Sci. 20 (2019) 1–23.
[11] C. Liu, W. Zhang, H. Yang, W. Sun, X. Gong, J. Zhao, A water-soluble inclusion complex of pedunculoside with the polymer β-cyclodextrin: a novel anti-inflammation agent with low toxicity, PLoS ONE 9 (2014), e101761.
[12] P.R. Krishna Mohan, G. Sreelakshmi, C.V. Muraleedharan, R. Joseph, Water-soluble complexes of curcumin with cyclodextrins: Characterization by FT-Raman spectroscopy, Vibr. Spectr. 62 (2012) 77–84.
[13] C.N. Murthy, K.E. Geckeler, The water-soluble β-cyclodextrin–[60]fullerene complex, Chem. Commun. (2001) 1194–1195.
[14] C. Borio, A. Zabai, Chapter 20: Unconventional monetary policies: a re-appraisal, Edward Elgar Publishing, 2018, pp. 398–444.
[15] Clinical Trials. gov (2020). Oseltamivir covid-19. Available at: ⟨https://clinicaltrials.gov/ct2/results?cond=Covid-19&term=Oseltamivir&cntry=&state=&city=&dist=⟩ (Accessed January 10, 2020).
[16] T. Higuchi, K.A. Connors, Phase solubility technique, Adv. Anal. Chem. Inst. 4 (1965) 117–212.
[17] R. Chadha, S. Gupta, N. Pathak, G. Shukla, D.V.S. Jain, R.R.S. Pissurlenkar, E. C. Coutinho, Binary and ternary complexes of arteether β-CD - characterization, molecular modeling and in vivo, Stud., Pharm. Pharm. 2 (2011) 212–225.
[18] Hyperchem, Hypercube, Inc., USA (2002) Hyperchem, Release 7.51 for windows 2002. Hypercube. Inc.
[19] J.C. Kromann, A.S. Christensen, C. Steinmann, M. Korth, J.H. Jensen, A third-generation dispersion and third-generation hydrogen bonding corrected PM6 method: PM6-D3H+, Peer. J. 2 (2014), e449.

[20] M. Fatiha, D.E. Khatmi, L. Largate, Theoretical approach in the study of the inclusion processes of sulconazole with Beta-cyclodextrin, J. Mol. Liq. 154 (2010) 1–5.
[21] L.J. Reed, H. Muench, A simple method of estimating fifty percent endpoints, Am. J. Hyg. 27 (1938) 493–497.
[22] M.E. Brewster, T. Loftsson, Cyclodextrins as pharmaceutical solubilizers, Adv. Drug. Deliv. Rev. 59 (2007) 645–666.
[23] A.B. Nair, M. Attimarad, B.E. Al-Dhubiab, J. Wadhwa, S. Harsha, M. Ahmed, Enhanced oral bioavailability of acyclovir by inclusion complex using hydroxypropyl-β-cyclodextrin, Drug Deli 21 (2014) 540–547.
[24] A. Saxena, G. Tewari, A. Saraf, Formulation and evaluation of mucoadhesive buccal patch of acyclovir utilizing inclusion phenomenon, Braz. J. Pharm. Sci. 47 (2011) 887–897.
[25] P. Mura, Analytical techniques for characterization of cyclodextrin complexes in aqueous solution: a review, J. Pharm. Biomed. Anal. 101 (2014) 238–250.
[26] M.A.M. Lyra, L.D.S. Alves, D.A.F. Fontes, J.L. Soares-Sobrinho, P.J. Rolim-Neto, Ferramentas analíticas aplicadas à caracterizaçã o de complexos de inclusão fármaco-ciclodextrina, Rev. Cienc. Farm. Basic. Apl. 31 (2010) 117–124.
[27] S. Yousuf, R. Alex, P.M. Selvakumar, I.M.V. Enoch, P.S. Subramanian, Y. Sun, Picking out logic operations in a naphthalene β-diketone derivative by using molecular encapsulation, controlled protonation, and DNA binding, ChemistryOpen 4 (2015) 497–508.
[28] J.C. de Miranda, T.E.A. Martins, F. Veiga, H.G. Ferraz, Cyclodextrins and ternary complexes: technology to improve solubility of poorly soluble drugs, Braz. J. Pharm. Sci. 47 (2011) 665–681.
[29] E. Iglesias, Inclusion complexation of novocaine by beta-cyclodextrin in aqueous solutions, J. Org. Chem. 71 (2006) 4383–4392.
[30] G. Tamil Selvan, S. Poomalai, S. Ramasamy, P.M. Selvakumar, I.V.M. Enoch, S. G. Lanas, A. Melchior, Differential metal ion sensing by an antipyrine derivative in aqueous and β-cyclodextrin media: selectivity tuning by β-cyclodextrin, Anal. Chem. 90 (2018) 13607–13615.
[31] J. Hernandez-Benito, M.P. García-Santos, E. O'Brien, E. Calle, J.J. Casado, A practical integrated approach to supramolecular chemistry III. thermodynamics of inclusion phenomena, J. Chem. Edu. 81 (2004) 540–545.
[32] M.S. Duan, N. Zhao, I.B. Ossurardottir, T. Thorsteinsson, T. Loftsson, Cyclodextrin solubilization of the antibacterial agents triclosan and triclocarban: formation of aggregates and higher-order complexes, Int. J. Pharm. 297 (2005) 213–222.
[33] J. Szejtli, Introduction and general overview of cyclodextrin chemistry, Chem. Rev. 98 (1998) 1743–1753.
[34] S. Saha, A. Roy, K. Roy, M.N. Roy, Study to explore the mechanism to form inclusion complexes of β-cyclodextrin with vitamin molecules, Sci. Rep. 6 (2016) 35764.
[35] H.A. Benesi, J.H. Hildebrand, A spectrophotometric investigation of the interaction of iodine with aromatic hydrocarbons, J. Am. Chem. Soc. 71 (1949) 2703–2707.
[36] M.N. Roy, A. Roy, A.S. Saha, Probing inclusion complexes of cyclodextrins with amino acids by physicochemical approach, Carb. Pol. 151 (2016) 458–466.
[37] J.S. Choi, J.C. Byeon, J.S. Park, Naftopidil-fumaric acid interaction in a solid dispersion system: improving the dissolution rate and oral absorption of naftopidil in rats, Mat. Sci. Eng. C. 95 (2019) 264–274.
[38] S. Manisha, K. Mamta, R. Swati, K.Y. Amit, R.S. Pratima, M. Subho, Influence of pH, β-Cyclodextrin, and Metal Ions on the Solubility and Stability of the Medicinally Competent Isoxazole Derivative of Curcumin: A Photophysical Study, ACS Appl. Biomater. 4 (2021) 8407–8423.
[39] P.S. Santos, L.K.M. Souza, T.S.L. Araujo, R. Jand Venes, S.C.C. Nunes, R. A. Carvalho, A.C.C. Pais, F.J.B. Veiga, L.C.C. Nunes, A. Figueiras, Methyl-β-cyclodextrin inclusion complex with β caryophyllene: preparation, characterization, and improvement of pharmacological activities, ACS Omega 2 (2017) 9080–9094.
[40] P.R. Krishna Mohan, G. Sreelakshmi, C.V. Muraleedharan, Roy Joseph, Water-soluble complexes of curcumin with cyclodextrins: Characterization by FT-Raman spectroscopy, Vibr. Spectr. 62 (2012) 77–84.
[41] C.J. Frank, in: M.J. Pelletier (Ed.), Analytical Applications of Raman Spectroscopy, Blackwell Science, United Kingdom, 1999, pp. 224–271.
[42] G. Narayanan, R. Boy, B.S. Gupta, A.E. Tonelli, Analytical techniques for characterizing cyclodextrins and their inclusion complexes with large and small molecular weight guest molecules, Pol. Test. 62 (2017) 402–439.
[43] P. Mura, Analytical techniques for characterization of cyclodextrin complexes in the solid state: a review, J. Pharm. Biomed. Anal. 113 (2015) 226–238.
[44] G. Fan, L. Zhang, Y. Shen, G. Shu, Z. Yuan, J. Lin, W. Zhang, G. Peng, Z. Zhong, L. Yin, H. Fu, Comparative muscle irritation and pharmacokinetics of for fenicolhydroxypropyl-β-cyclodextrin inclusion complex freeze-dried powder injection and florfenicol commercial injection in beagle dogs, Sci. Rep. 9 (2019) 16739.
[45] A. Celebioglu, T. Uyar, Fast dissolving oral drug delivery system based on electrospun nanofibrous webs of cyclodextrin/ibuprofen inclusion complex nanofibers, Mol. Pharm. 16 (2019) 4387–4398.
[46] A. Celebioglu, T. Uyar, Development of ferulic acid/cyclodextrin inclusion complex nanofibers for fast-dissolving drug delivery system, Int. J. Pharm. 584 (2020), 119395.
[47] G.A. El-Emam, G.N.S. Girgis, M.M.A. El Sokkary, O.A. El- Azeem Soliman, A.E.G. H. Abd El Gawad, Ocular inserts of voriconazole-loaded proniosomal gels: formulation, evaluation and microbiological studies, Int. J. Nanomed. 15 (2020) 7825–7840.
[48] P. Siafaka, P. Barmpalexis, D.N. Bikiaris, Novel electrospun nanofibrous matrices prepared from poly(lactic acid)/poly(butylene adipate) blends for controlled release formulations of an anti-rheumatoid agent, Eur. J. Pharm. Sci. 88 (2016) 12–25.
[49] R. Periasamy, S. Kothainayaki, R. Rajamohan, K. Sivakumar, Spectral investigation and characterization of host-guest inclusion complex of 4,4′-methylene-bis(2-chloroaniline) with beta-cyclodextrin, Carb. Pol. 114 (2014) 558–566.
[50] K. Srinivasan, K. Kayalvizhi, K. Sivakumar, T. Stalin, Study of inclusion complex of β-cyclodextrin and diphenylamine: photophysical and electrochemical behaviors, Spectrochim. Acta Part A 79 (2011) 169–178.
[51] R. Periasamy, R. Rajamohan, S. Kothainayaki, K. Sivakumar, Spectral investigation and structural characterization of dibenzalacetone: β-Cyclodextrin inclusion complex, J. Mol. Str. 1068 (2014) 155–163.
[52] R. Periasamy, S. Kothainayaki, K. Sivakumar, Preparation, physicochemical analysis and molecular modeling investigation of 2,2′-Bipyridine: β-Cyclodextrin inclusion complex in solution and solid state, J. Mol. Str. 1100 (2015) 59–69.
[53] T. Wanjun, L. Yuwen, Z. Hen, W. Zhiyong, W. Cunxin, New temperature integral approximate formula for non-isothermal kinetic analysis, J. Therm. Anal. Cal. 74 (2003) 309–315.
[54] F. Topuz, M.E. Kilic, E. Dugun, G. Szekely, Fast dissolving antibacterial nanofibers of cyclodextrin/antibiotic inclusion complexes for oral drug delivery, J. Coll. Inter. Sci. 585 (2021) 184–194.
[55] G.G.G. Trindade, G. Thrivikraman, P.P. Menezes, C.M. França, B.S. Lima, Y.M.B. G. Carvalho, E.P.B.S.S. Souza, M.C. Duarte, S. Shanmugam, L.J. Quintans-Júnior, D.P. Bezerra, L.E. Bertassoni, A.A.S. Araújo, Carvacrol/β-cyclodextrin inclusion complex inhibits cell proliferation and migration of prostate cancer cells, Food Chem. Toxic. 125 (2019) 198–209.
[56] Z. Éhen, F. Giordano, J. Sztatisz, L. Jicsinszky, C.S. Novák, Thermal characterization of natural and modified cyclodextrins using TG-MS combined technique, J. Therm. Anal. Calor. 80 (2005) 419–424.
[57] S. Uppal, K. Kaur, Rajendra Kumar, N.K. Kaur, Rachna Singh, S.K. Mehta, Encompassment of Benzyl Isothiocyanate in cyclodextrin using ultrasonication methodology to enhance its stability for biological applications, Ultrason. Sonochem. 39 (2017) 25–33.
[58] A. Figueiras, R.A. Carvalho, L. Ribeiro, J.J. Torres-Labandeira, F.J.B. Veiga, Solid-state characterization and dissolution profiles of the inclusion complexes of omeprazole with native and chemically modified β-cyclodextrin, Eur. J. Pharm. Biopharm. 67 (2007) 531–539.
[59] S. Bekiroglu, A. Sandström, L. Kenne, C. Sandström, Ab initio and NMR studies on the effect of hydration on the chemical shift of hydroxy protons in carbohydrates using disaccharides and water/methanol/ethers as model systems, Org. Biomol. Chem. 2 (2004) 200–205.
[60] A.N. Bristol, J. Saha, H.E. George, P.K. Das, L.K. Kemp, W.L. Jarrett, V. Rangachari, S.E. Morgan, Effects of stereochemistry and hydrogen bonding on glycopolymer-amyloid-β-interactions, Biomacromol 21 (2020) 4280–4293.
[61] P.K. Das, D.N. Dean, A.L. Fogel, F. Liu, B.A. Abel, C.L. McCormick, E. Kharlampieva, V. Rangachari, S.E. Morgan, Aqueous RAFT synthesis of glycopolymers for determination of saccharide structure and concentration effects on amyloid β-aggregation, Biomacromol 18 (2017) 3359–3366.
[62] M. Szöri, P. Jedlovszky, M. Roeselová, Water adsorption on hydrophilic and hydrophobic self-assembled monolayers as proxies for atmospheric surfaces. A grand canonical Monte Carlo simulation study, Phys. Chem. Chem. Phys. 12 (2010) 4604–4616.
[63] M.N. Martinez, A.G. Smith, L.M. Nowack, B. Lin, S.A. Rice, Interaction between dilute water vapor and dodecane thiol ligated Au nanoparticles: Hydrated structure and pair potential of mean force, J. Chem. Phys. 155 (2021), 144902.
[64] M.J. Webber, E.A. Appel, E.W. Meijer, R. Langer, Supramolecular biomaterials, Nat. Mat. 15 (2016) 13–26.
[65] M.J. Webber, R. Langer, Drug delivery by supramolecular design, Chem. Soc. Rev. 46 (2017) 6600–6620.
[66] P. Evenou, J. Rossignol, G. Pembouong, A. Gothland, D. Colesnic, R. Barbeyron, S. Rudiuk, A.-G. Marcelin, M. Ménand, D. Baigl, V. Calvez, L. Bouteiller, M. Sollogoub, Bridging β-cyclodextrin prevents self-inclusion, promotes supramolecular polymerization, and promotes cooperative interaction with nucleic acids, Ang. Chem. Int. Ed. 57 (2018) 7753–7758.